Journal of Molecular Catalysis A: Chemical 304 (2009) 128–134

Contents lists available at ScienceDirect

Journal of Molecular Catalysis A: Chemical

journal homepage: www.elsevier.com/locate/molcata

Effect of Mo addition on precipitated Fe catalysts for Fischer–Tropsch synthesis

Shaodong Qin[a,b], Chenghua Zhang[a,*], Jian Xu[a], Baoshao Wu[a], Hongwei Xiang[a], Yongwang Li[a]

[a] State Key Laboratory of Coal Conversion, Institute of Coal Chemistry, Chinese Academy of Sciences, Taoyuan South Road 27#, Taiyuan 030001, People's Republic of China
[b] Graduate University of Chinese Academy of Sciences, Beijing 10039, People's Republic of China

ARTICLE INFO

Article history:
Received 21 October 2008
Received in revised form 16 January 2009
Accepted 1 February 2009
Available online 10 February 2009

Keywords:
Fischer–Tropsch synthesis
Precipitated iron-based catalysts
Mo promotion
Hydrocarbon selectivivity

ABSTRACT

Effects of Mo addition on the performance of precipitated Fe catalysts for Fischer–Tropsch synthesis (FTS) were studied in a slurry reactor at 280 °C, 1.5 MPa, 2000 h^{-1}, and syngas $H_2/CO = 1.2$. The catalysts were characterized by N_2 adsorption, H_2 or CO temperature programmed reduction (TPR), NH_3 temperature programmed desorption (TPD), X-ray diffraction (XRD), and Mössbauer effect spectroscopy (MES). It was found that there is a strong interaction between Fe and Mo, which inhibited the reduction and carburization of Fe catalyst. The surface acidity of the catalysts was also found to increase with addition of molybdenum. In the FTS process, Mo addition decreased the FTS activity of Fe catalyst, markedly enhanced C_{12}^+ hydrocarbon selectivity, while suppressed C_2–C_8 hydrocarbon selectivity as validated by non-ASF product distribution curves.

1. Introduction

Depleting oil reserves and environmental constrains make it necessary to develop new technologies and processes for synthesizing ultra-clean hydrocarbon fuels. The Fischer–Tropsch synthesis (FTS), first developed in Germany in 1923 [1] and now practiced in large scale in SASOL and Shell, is considered to be an efficient route for converting syngas into transportation fuels and useful chemicals. Iron-based catalysts receive a persistent research interest due to its water–gas-shift activity as well as its easy availability and low cost. The polymerization-type nature of FT synthesis, however, determines the products spectrum following the Anderson–Schulz–Flory (ASF) distribution and a poor selectivity to specific hydrocarbon fraction. Therefore, research attempts to enhance fuel selectivity and break the ASF limitation were made with addition of chemical and structural promoters such as K [2,3], Cu [4], Mn [5,6] and zeolite [7,8] into the iron-based catalysts.

Many factors have influences on the hydrocarbon selectivity of iron-based catalysts. For instance, potassium promoted catalysts can produce more heavy hydrocarbons. Reactions under lower H_2/CO ratio, lower temperature and higher pressure can obtain more wax products. These factors, however, do not change the ASF distribution. The composite catalysts of a FT component and a zeolite exhibit the acid-catalyzed reactions such as isomerization, oligomerization and cracking, which can circumvent the ASF distribution to some extent, while the higher coking tendency on acid sites of zeolite deteriorates the stability of catalysts [8]. Molybdenum has been reported to be moderately active for FTS, but very selective to light hydrocarbons [9–11]. Schultz et al. [9] first investigated the catalytic performance of molybdenum. In comparison to Group VIII metals, they concluded that Mo had moderate activity in CO hydrogenation. Afterwards, Murchison and Murdick [10] reported a new supported Mo catalyst promoted with alkali which converted more than 70% syngas to LPG and showed high sulfur resistance and low rate of coking at high temperature. The recent quantum chemistry calculation results [12] have proved that using Mo as promoter could increase the activation of CO and sulfur poisoning tolerance for Fe catalyst. Molybdenum carbides are well-known catalysts as substitutes of noble metals in hydrogenation and isomerization reactions [13–15]. Moreover, the intrinsic acid sites on molybdenum oxides or carbides could catalyze olefin oligomerization or wax cracking reactions. Therefore, it could be expected that molybdenum addition to traditional iron catalyst might have potential advantages to selective production of high quality liquid fuels in one-step FTS reaction.

More recently, Ma et al. [16] investigated the Mo loading Fe catalysts supported on activated carbon and found that Mo addition greatly enhanced secondary reactions of olefins. The Mo oxide used as a promoter/additive to precipitated Fe catalysts, however, has rarely been reported. The present work was carried out to study the effect of molybdenum on the catalytic behavior of the precipitated Fe catalyst. Incorporation manner of molybdenum and the results of reaction evaluations in slurry phase continuously stirred tank reactor (CSTR) were discussed.

* Corresponding author. Tel.: +86 351 7560127; fax: +86 351 7560668.
E-mail address: zhangchh@sxicc.ac.cn (C. Zhang).

1381-1169/$ – see front matter © 2009 Elsevier B.V. All rights reserved.
doi:10.1016/j.molcata.2009.02.001

2. Experiment

2.1. Catalyst preparation

The iron-based catalyst precursors were prepared from precipitation of a $Fe(NO_3)_3$ (99.9+%) solution using aqueous ammonia as the precipitating agent. Under continuously stirring, the iron nitrate and ammonia solutions were simultaneously added into the precipitated vessel maintained at a constant pH value of 9.0 ± 0.1. The obtained iron precipitate was then filtered, washed and divided into three parts. For one part, silica sol was subsequently incorporated with vigorous agitating. After drying in air at 120 °C for 24 h, desired amount of Mo was added by aqueous impregnation of $(NH_4)_6Mo_7O_{24}$ (99.9+%). The resulting oxide was denoted as Mo5-1/Fe. For the other two parts, one was mixed with silica sol to obtain the Mo-free sample Mo00/Fe, while the other was mixed with a silica sol and $(NH_4)_6Mo_7O_{24}$ solution to get the catalyst Mo5-2/Fe. After incorporating silica and/or molybdenum, all the catalyst precursors were promoted with potassium using K_2CO_3 (99.9+%) as K source. At last, the precursors were calcined at 500 °C for 5 h to obtain the final catalysts. The composition of the final catalysts were $100Fe/x Mo/1.5K/15SiO_2$ in mass basis ($x = 0, 5$).

2.2. Catalyst characterization

The BET surface area, pore volume and average pore diameter of the fresh catalysts were obtained from the nitrogen physisorption at −196 °C in ASAP 2420 (Micromeritics, USA). Each sample was degassed under vacuum at 90 °C for 1 h and 350 °C for 8 h prior to the measurement.

Powder X-ray diffraction (XRD) patterns were obtained with a D/max-RA X-ray diffratometer (Rigaku, Japan), equipped with Cu Kα radiation ($\lambda = 1.5406$ Å) at 40 kV and 150 mA. The Mössbauer effect spectroscopy (MES) experiments were carried out in a CANBERRA series 40 MCA constant-acceleration drive with a triangular reference signal at room temperature. The radioactive source was a 25 mCi ^{57}Co in Pd matrix. Data analysis was performed using a nonlinear least squares fitting routine that models the spectra as a combination of singlets, quadruple doublets, and magnetic sextets based on a Lorentzian line shape profile. The components were identified based on their isomer shift (IS), quadruple splitting (QS), and magnetic hyperfine field (Hhf). Magnetic hyperfine fields were calibrated with the 330 kOe field of α-Fe at the ambient temperature.

Temperature programmed reduction (TPR) studies were carried out on Auto chem. II 2920 equipment (Micromeritics, USA). 40 mg catalyst was loaded in a U-type quartz tube reactor and ramped from room temperature to 1000 °C in 10% H_2/90% Ar (H_2-TPR) or in 5% CO/95% He (CO-TPR). The heating rate was maintained at 6 °C/min and flow rate at 50 mL/min. The variation of the reducing gas concentration was monitored by a thermal conductivity detector (TCD). Isopropyl alcohol gel (−88 °C) and liquid nitrogen trap were respectively used to remove water (in H_2-TPR) and CO_2 (in CO-TPR) formed during tests. In order to quantify the degree of reduction in H_2-TPR, H_2 consumption during reduction of CuO oxides under the same TPR procedures was used as a calibration standard for peak areas.

NH_3 temperature programmed desorption (TPD) was conducted in the same equipment as that of TPR. 100 mg sample was pretreated in He at 450 °C for 60 min, and then cooled to 100 °C. Subsequently, the catalyst was flushed with pure NH_3 at 100 °C for 30 min, purged with He for 30 min and heated to 450 °C at 10 °C/min.

Table 1
Textural property of the fresh catalysts.

Catalyst	Mo00/Fe	Mo5-1/Fe	Mo5-2/Fe
Specific area (m^2/g)	202.95	184.07	183.57
Pore volume (cm^3/g)	0.424	0.405	0.371
Average pore diameter (nm)	6.69	7.17	6.45

2.3. Catalysts evaluation

FTS testing was conducted in a 1 L continually stirred tank reactor (CSTR) loaded with 10 g catalyst sample and 380 g liquid paraffin. The H_2 and CO were passed through two purification series separately to remove any impurities. The flow rates of the gases were controlled by mass flow meters separately (5850E, Brooks). And the flow rate of the tail gas was measured by a wet-gas flow meter. The tail gas was analyzed on-line by gas chromatographs (GC) (models 6890N and 4890D; Agilent). The liquid sample was withdrawn every 24 h and analyzed on an off-line GC (models 6890N, Agilent). The detailed description of the reactor and product analysis system has been provided elsewhere [17].

Catalysts were pretreated in situ with syngas ($H_2/CO = 0.7$) at 280 °C, 0.5 MPa, 1000 h^{-1} for 30 h. After the pretreatment, the reaction conditions were adjusted to 280 °C, 2000 h^{-1}, 1.5 MPa, and $H_2/CO = 1.2$ for FTS performance measurement.

3. Result and discussion

3.1. Surface properties of catalysts

The BET surface area, pore volume and average pore diameter of catalysts are illustrated in Table 1. It is evident that Mo addition results in a decrease in both the BET surface area and the total pore volume of the precipitated Fe catalyst. The average pore diameter of Mo5-1/Fe is larger than Mo-free sample Mo00/Fe while that of Mo5-2/Fe is smaller. Similarly, the pore size distribution (PSD) in Fig. 1 shows a larger pore diameter in the Mo5-1/Fe catalyst, indicating that the small pores of precursor Fe/SiO_2 were blocked when Mo was added by impregnation. But for the Mo5-2/Fe catalyst in which Mo was incorporated with binder SiO_2, the PSD curve shifts to smaller pore diameter compared with the Mo00/Fe catalyst, suggesting that Mo addition in this manner can lower the pore size of Fe/SiO_2 catalyst.

The effect of Mo addition on the surface acidity of Fe catalyst was studied by NH_3-TPD. The profiles of NH_3 desorption are shown in Fig. 2. Two overlapped peaks are shown in the profiles; the first

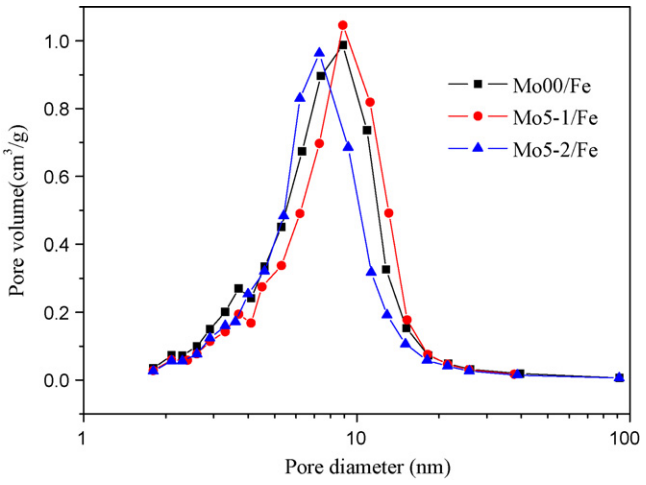

Fig. 1. The pore size distribution of catalysts as prepared.

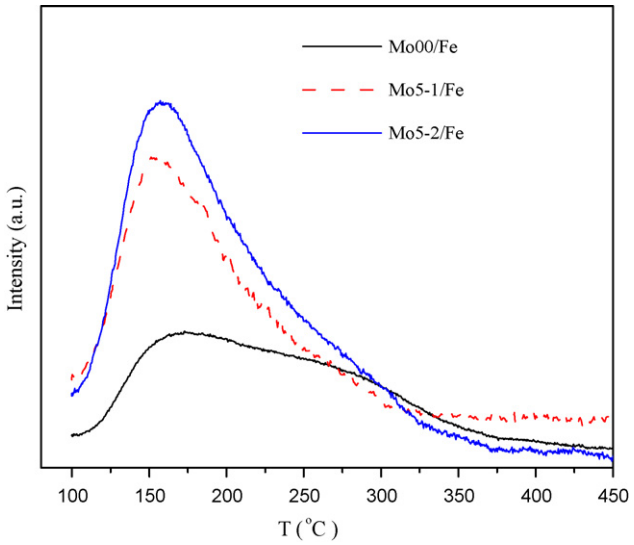

Fig. 2. NH_3-TPD profiles of the catalysts as prepared.

peak at about 160 °C (peak 1) corresponds to the desorption of NH_3 from weak acid sites on catalysts surface, while the second peak at the temperature about 260 °C (peak 2) can be ascribed to the desorption of NH_3 from stronger acid sites. The intensities of desorption peaks increase with the addition of Mo, in orders of Mo5-2/Fe > Mo5-1/Fe > Mo00/Fe. Due to the decreased surface areas with Mo addition as validated by N_2 physisorption, we can speculate that the increased surface acidity is largely resulted from the Mo addition.

3.2. Crystallite structure of the catalysts

3.2.1. Catalysts as prepared

The XRD patterns of catalysts as prepared are presented in Fig. 3(a). All the XRD patterns show broad diffractogram with several diffraction peaks at 2θ values of 24.2°, 33.2°, 35.6°, 62.48° and 63.4°, all of which are the characteristic of hematite (α-Fe_2O_3). No Mo phase is presented in the XRD patterns of the Mo-added catalysts, indicating that Mo elements are highly dispersed on catalysts. In comparison with the Mo00/Fe catalyst, the hematite characteristic peaks of Mo5-1/Fe catalyst show stronger in intensities, while those of Mo5-2/Fe catalyst become weaker. This suggests that impregnated Mo inhibits the dispersion of iron oxide, whereas the Mo incorporated with SiO_2 facilitates the dispersion of iron oxide to a lesser extent, which is in agreement with the results of N_2 physisorption. It was reported that the mixture of Fe_2O_3 and MoO_3 can form a ferric molybdate ($Fe_2(MoO_4)_3$) when calcined at temperature above 470 °C [18]. However, in this study, SiO_2 plays a dominate role in catalysts so that it is difficult to clearly distinguish the existence of different iron and/or molybdenum oxide phases. To distinguish the phases in catalysts, a model Fe–Mo sample (100Fe/25Mo, weight ratio) without silica was prepared and characterized by XRD. As shown in Fig. 3(a), characteristic peaks of α-Fe_2O_3 and $Fe_2(MoO_4)_3$ are both presented in the diffractogram of the model sample. With the same preparation and pretreatment processes, the ferric molybdate phase exists in the Mo-added catalysts at a large possibility.

3.2.2. Catalysts after activation and FTS reaction

After reduction with syngas (H_2/CO = 0.67) at 280 °C for 30 h, the phase compositions of catalysts were determined by XRD and MES. In the XRD patterns, as shown in Fig. 3(b), only the characteristic peaks of magnetite (Fe_3O_4) can be seen, and the peak intensities

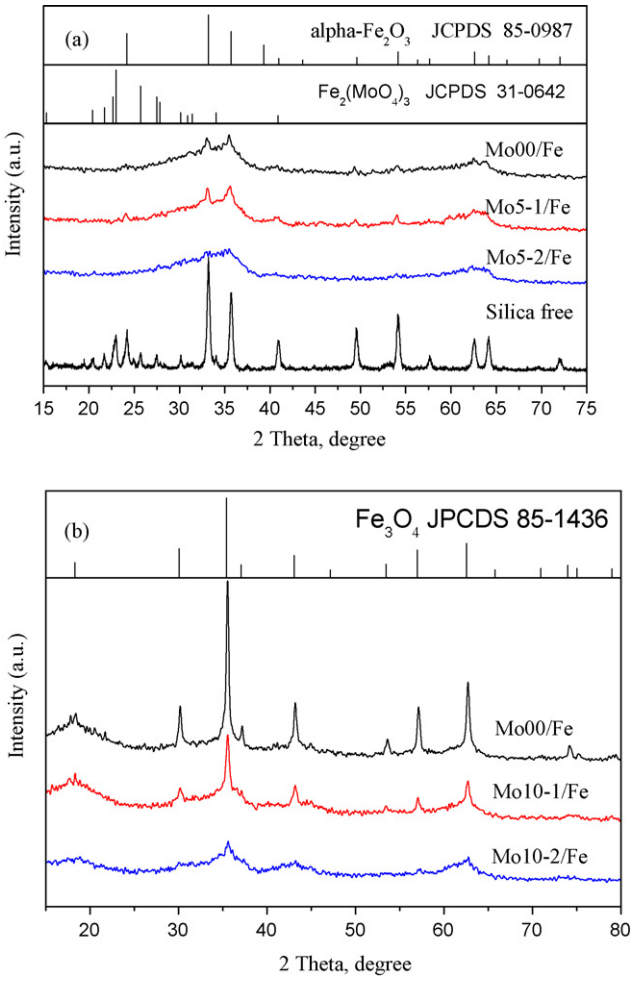

Fig. 3. XRD patterns of samples (a) as prepared (b) after reduction.

decrease in order of Mo00/Fe > Mo5-1/Fe > Mo5-2/Fe. Probably due to the poor crystallographic form and very limited amount, no iron carbides peaks can be seen in the diffractograms. The MES spectra of catalysts after reduction are presented in Fig. 4(a). The spectrum parameters and the corresponding iron phase compositions are summarized in Table 2. The MES results indicate that the main phases of Mo-free sample (Mo00/Fe) are Fe_3O_4 (36.9%), superparamagnetic (spm) Fe^{2+} (37.5%) and Fe^{3+} (20.3%). With Mo addition, spm Fe^{3+} and Fe^{2+} are the dominating iron species. The content

Table 2
Mössbauer parameters of catalysts after reduction.

Catalysts	Phases	Mössbauer parameters			
		IS (mm/s)	QS (mm/s)	Hhf (kOe)	Area (%)
Mo00/Fe	χ-Fe_5C_2	0.33	0.18	217	5.2
	Fe_3O_4	0.66	−0.03	458	26.1
		0.28	−0.01	489	10.8
	Fe^{3+}	0.37	0.81		37.5
	Fe^{2+}	0.97	1.50		20.3
Mo5-l/Fe	χ-Fe_5C_2	0.36	0.16	225	2.9
	Fe_3O_4	0.69	−0.07	456	11.3
		0.25	0.04	488	2.8
	Fe^{3+}	0.37	0.81		53.3
	Fe^{2+}	0.89	1.61		29.6
Mo5-2/Fe	Fe_3O_4	0.35	0.02	484	2.5
	Fe^{3+}	0.35	0.77		34.5
	Fe^{2+}	0.91	1.46		62.6

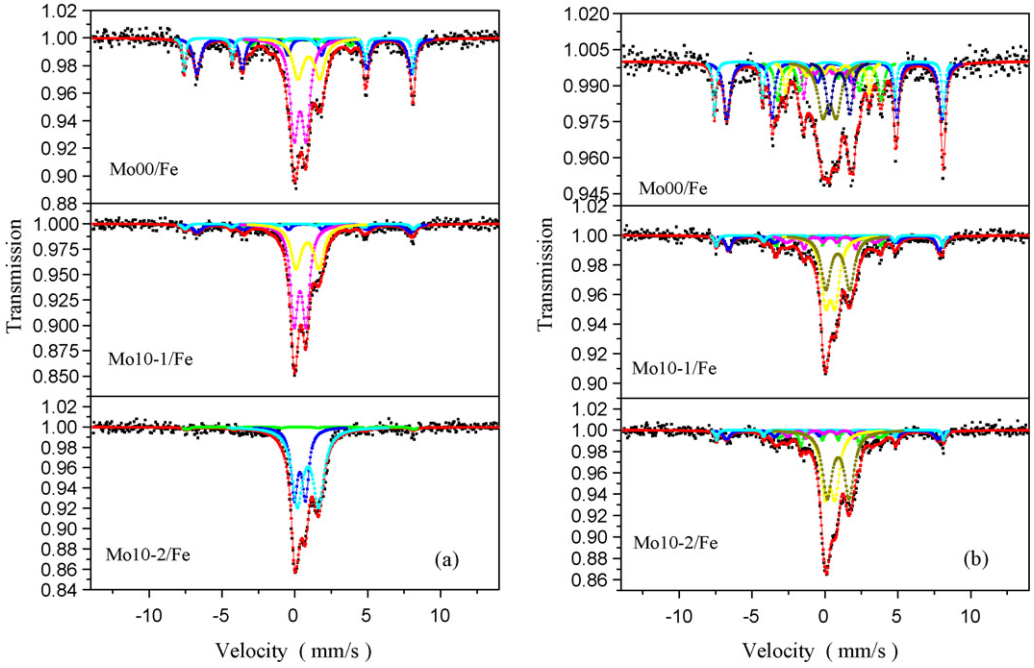

Fig. 4. Mössbauer spectra of the catalysts after reduction (a) and after FTS reaction (b).

of Fe_3O_4 decreases to 14.1% for Mo5-1/Fe and 2.5% for Mo5-2/Fe, which is in good agreement with XRD results. In Mo00/Fe, 5% iron carbide (χ-Fe_5C_2) is detected, but in Mo5-1/Fe the carbide contribution decreases to 2.5% and no carbide is detected in Mo5-2/Fe after reduction. These results indicate that the Mo addition suppresses the reduction and carburization of iron oxide. Moreover, the Mo incorporated during the re-slurrying process has much more apparent effect on the reduction/carburization than the impregnated Mo.

The MES spectra of catalysts after 200 h reaction are shown in Fig. 4(b) and the spectra parameters are listed in Table 3. Comparison with the reduced samples, it can be found that the contents of χ-Fe_5C_2 and Fe_3O_4 increase while the amounts of spm Fe^{3+} and Fe^{2+} decrease, suggesting that the catalysts were further reduced and carburized during the FTS reaction. In Mo00/Fe, the spectral contribution of χ-Fe_5C_2 is about 35%, but that is 16.9% in Mo5-1/Fe and 11.1% in Mo5-2/Fe, further indicating that the presence of Mo can greatly inhibits the formation of iron carbide.

Table 3
Mössbauer parameters of catalysts after FTS.

Catalysts	Phases	Mössbauer parameters			
		IS (mm/s)	QS (mm/s)	Hhf (kOe)	Area (%)
Mo00/Fe	χ-Fe_5C_2	0.31	−0.01	220	15.8
		0.31	−0.26	179	9.8
		0.28	−0.02	106	8.1
	Fe_3O_4	0.66	0.01	459	26.7
		0.28	−0.01	489	11.9
	Fe^{3+}	0.31	0.93		16.8
	Fe^{2+}	1.00	1.42		10.8
Mo5-l/Fe	χ-Fe_5C_2	0.36	0.16	223	6.3
		0.37	0.06	190	10.6
	Fe_3O_4	0.67	−0.11	450	12.4
		0.30	0.01	483	4.9
	Fe^{3+}	0.38	0.66		34.3
	Fe^{2+}	0.89	1.63		34.6
Mo5-2/Fe	χ-Fe_5C_2	0.34	−0.07	216	11.1
		0.35	−0.03	180	5.3
	Fe_3O_4	0.63	−0.24	451	8.5
		0.34	0.05	484	3.7
	Fe^{3+}	0.36	0.69		31.9
	Fe^{2+}	0.92	1.51		39.4

3.3. Reduction and carburization behaviors

Catalysts reduction and carburization behaviors were studied by H_2-TPR and CO-TPR. The H_2-TPR profiles are shown in Fig. 5 and the amounts of H_2 consumed at different stages are listed in Table 4. As shown in Fig. 5, the profile of Mo00/Fe shows two broad reduction peaks at about 373 °C and 555 °C, and the latter is also accompanied by a shoulder at the higher temperature side. The hydrogen consumption for the first peak is 0.5 mol H_2/mol Fe, corresponding to the reduction of Fe_2O_3 to FeO. The second peak and the shoulder, accordingly, can be attributed to the reduction of FeO to α-Fe. In the profiles of Mo promoted catalysts Mo5-1/Fe and Mo5-2/Fe, two main reduction peaks are also observed. But the hydrogen consumption of the first peak (0.28 mol H_2/mol Fe for Mo5-1/Fe and 0.31 mol H_2/mol Fe for Mo5-2/Fe) is not consistent with theoreti-

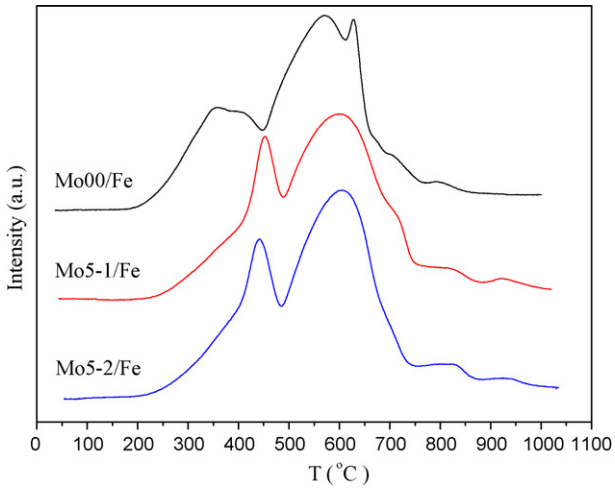

Fig. 5. H_2-TPR profiles of the catalysts.

Table 4
Quantitative results of H_2 consumption in H_2-TPR process.

Catalyst samples	Peak (°C)	H_2 consumption (mol H_2/mol Fe)	Total H_2 consumption (μmol)
Mo00/Fe	373.0	0.50	0.61
	555.0	0.71	
	629.7	0.15	
	444.2	0.28	
Mo5-1/Fe	586.5	1.12	0.63
	796.6	0.05	
	911.9	0.02	
	438.1	0.31	
Mo5-2/Fe	598.1	1.05	0.66
	796.0	0.16	
	922.0	0.03	

cal value of reduction from Fe_2O_3 to Fe_3O_4 (0.17 mol H_2/mol Fe) or Fe_2O_3 to FeO (0.5 mol H_2/mol Fe), indicating that part of Fe_2O_3 has been reduced to Fe_3O_4 and the rest has been reduced to FeO. Correspondingly, the second peak of the samples can be ascribed to the reduction of Fe_3O_4 and FeO to α-Fe. It should be noted that if the H_2 uptakes of Mo oxide is taken into account in the first reduction step, the hydrogen consumption is close to the theoretical value of reduction from Fe_2O_3 and MoO_3 to Fe_3O_4 and Mo metal (0.31 mol H_2/mol M, M = Fe + Mo). But the possibility can be exclude because Mo oxide of low valence or the metal cannot be obtained at the reduction temperature [19,20].

Results of H_2-TPR show that Mo addition has an evident effect on the reduction behavior of Fe catalysts. 5% Mo addition shifts the reduction peaks to high temperature, especially for the first peak from 373 °C to about 440 °C. Moreover, in the first reduction stage only part of Fe_2O_3 has been reduced to FeO unlike the Mo-free sample in which Fe_2O_3 are reduced to FeO completely. All these results suggest a strong interaction between Fe and Mo which suppresses the reduction of iron oxide. It is in accord with the study of Ma et al. [16], in which Mo addition inhibited the iron reduction of catalysts supported on activated carbon in dilute hydrogen. Table 4 also shows a minor increase in the overall H_2 consumption of catalysts with Mo promotion probably due to the part reduction of Mo oxide in the TPR process.

CO-TPR profiles of the catalysts are shown in Fig. 6. All catalysts present two well-separated peaks in CO-TPR curves which are characteristic of two-step reduction of Fe_2O_3 to Fe_3O_4 and Fe_3O_4 to carbides in CO atmosphere [21]. The addition of Mo obviously suppresses the reduction and carburization of catalysts, leading to

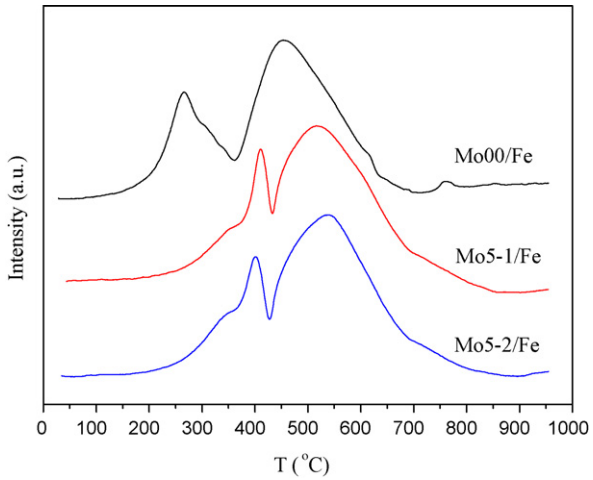

Fig. 6. CO-TPR profiles of the catalysts.

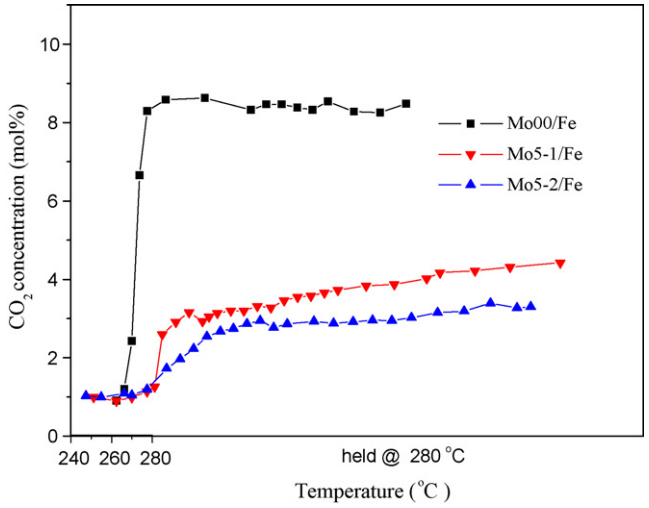

Fig. 7. The change of CO_2 concentration in tail gas during reduction process; reduction condition: 280 °C, H_2/CO = 0.7, 0.5 MPa, 1000 h^{-1} for 30 h.

the presence of CO consumption peaks at high temperature. For instance, the temperature of the first reduction peak shifts from 262 °C to 400 °C and above with Mo addition. Moreover, a long tail at high temperature is also observed on the profiles of Mo-added catalysts. These results are similar to those observed in H_2-TPR, suggesting that Mo addition inhibits the reduction and/or carburization behaviors of iron oxides either in H_2 or in CO.

The reduction behaviors of catalysts in syngas (H_2/CO = 0.67, v/v) are shown in Fig. 7 as the change of CO_2 concentration in the tail gas during the in situ pretreatment, which can monitor the reduction extent of catalysts or the formation of FTS active phases. With increasing reduction temperature to 280 °C, as shown in Fig. 7, the CO_2 concentration of Mo00/Fe rapidly increases to a much higher level (ca. 8.5%) and keeps constant. However, the CO_2 concentrations of Mo5-1/Fe and Mo5-2/Fe catalysts show a slow and gradual ascending tendency at the low concentration level, which also suggests the inhibitive effect of Mo on the reduction of catalysts in syngas. Comparing the two addition manners of Mo, it can be found that the CO_2 concentration of Mo5-1/Fe is slightly higher than that of Mo5-1/Fe during the whole reduction process. It is consistent with the composition analysis of XRD and MES which indicate a higher reduction extent for Mo5-1/Fe catalyst than that for Mo5-2/Fe catalyst.

TPR studies and tail gas analysis during reduction process indicate that Mo promoter inhibits the reduction/carburization of iron oxide. It is in agreement with the of bulk phase analysis with XRD and MES of catalysts after activation and FTS reaction. One aspect of the inhibitive effect of Mo on the reduction/carburization of iron oxide is due to the poor reducibility of molybdenum oxides. Higher activation energies (80–190 kJ/mol) of the reduction MoO_3 to MoO_2 [19] were reported than those (74–117 kJ/mol) of Fe_2O_3 to Fe_3O_4 [22,23]. The reduction/carburization process of iron oxides generally includes the removal of O atoms from oxide phase and the carburization of C atoms into the interstitial vacancies of iron phase. With addition of Mo, the Fe-catalyzed H_2 or CO dissociation sites on iron oxide surface are covered by molybdenum oxides so that the surface active H or C reducing agents are greatly decreased. Thus, the reductions of Mo-added catalysts shift to high temperature. Another aspect of the inhibitive effect of Mo is the formation of a reduction-resistant phase $Fe_2(MoO_4)_3$. Zhang et al. [24] had studied the reduction behavior of Fe–Mo–O catalysts using TPR and found that the $Fe_2(MoO_4)_3$ phase was initially reduced at temperature above 580 °C and completely reduced to metallic Fe and Mo at temperature above 960 °C in the TPR process, which is

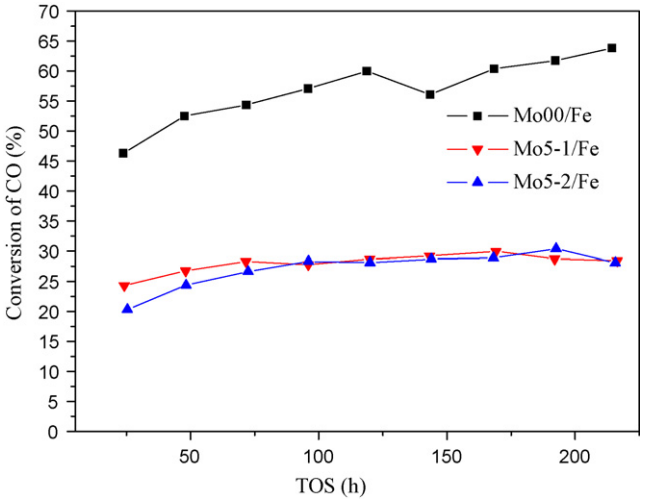

Fig. 8. Effect of Mo promotion on the activity of Fe catalyst; reaction conditions: 280 °C, $H_2/CO = 1.2$, 1.5 MPa, 2000 h^{-1}.

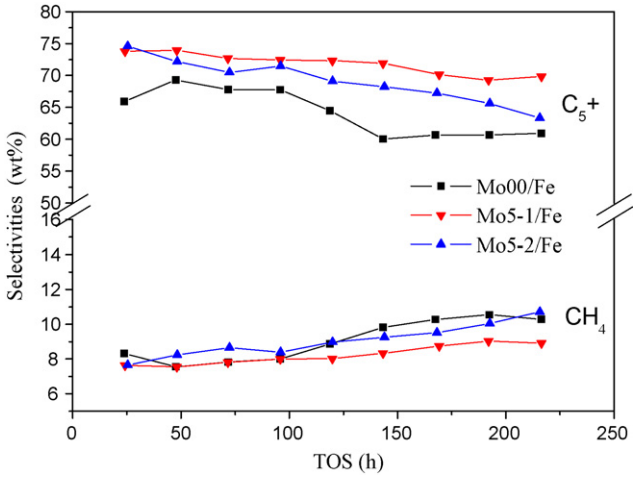

Fig. 9. Effect of Mo addition on the selectivities of CH_4 and C_5^+.

higher than the temperatures required for the reduction of iron oxide or molybdenum oxide. Although the phase of $Fe_2(MoO_4)_3$ was not detected in the Mo-added catalysts due to the dispersion of silica, the deteriorated reducibility of catalysts with Mo addition is possibly resulted from the difficultly reduced $Fe_2(MoO_4)_3$ phase. Comparison of the Mo additions, the Mo5-2/Fe catalyst, in which Mo was added with silica during the re-slurrying process, has more intimate interaction between iron and molybdenum than the Mo5-1/Fe catalyst with Mo impregnated on Fe/SiO_2 precursors. The Mo5-2/Fe catalyst contains the ferric molybdate phase at larger possibility or in larger amount than the Mo5-1/Fe catalyst. Thus, it is reasonable for the lower reduction/carburization extent of the Mo5-2/Fe catalyst. However, the Mo addition manners have little effect on the reduction/carburization behaviors of iron oxides relative to the easy reducibility of the Mo00/Fe catalyst. Thus, it can be seen that the intrinsic low reducibility of molybdenum oxide maybe plays a critical role in inhibiting the reduction of iron oxides.

3.4. Activity and selectivity

3.4.1. Catalyst activities

The effects of Mo on the FTS activity of catalysts in CO conversion are shown in Fig. 8. For Mo00/Fe catalyst, the CO conversion is at a high level (46%) at the beginning of the reaction and continually increases with time on stream (TOS). At 200 h the conversion is higher than 60%. On Mo promoted catalysts Mo5-1/Fe and Mo5-2/Fe, however, the CO conversions are initially lower than 25%, and then gradually increase to 30% during the first 100 h and maintain stable. It is worth noting that the CO conversion of Mo5-2/Fe is initially in a lower level than Mo5-1/Fe but increase faster in the next 100 h, and finally reaches the same level as that of Mo5-2/Fe and remains stable. The results indicate that the incorporation manners have little effect on the activity of catalysts.

It is obvious that Mo addition markedly decreases the activity of catalysts due to the inhibitive effect of Mo on the formation of active phases (iron carbides) as validated by TPR, XRD and MES analysis. However, the study of Ma et al. [16] showed that the activity of Fe–Cu–K catalyst supported on activated carbon was increased when 6% Mo was added. Recently, Lohitharn et al. [25] systematically studied the impact of addition different transition metal, such as Cr, Mn, Mo, Ta, etc., on the properties of a Fe-based catalyst and also found that Mo addition increased the FTS activity of Fe–Cu–K catalyst. This discrepancy might be related to the difference in catalyst composition or preparation, most probably due to the presence of reduction promoter Cu in their catalysts. It is known that Cu could improve the reduction of Fe catalyst and enhanced the activity [17]. Thus, the suppression of the FTS activity on Fe catalyst with Mo addition should also be offset by Cu addition. For further study, the Cu promotion effect on the Fe–Mo system will be systematically studied in our group.

3.4.2. Product selectivity

The changes of methane and high-molecular-weight hydrocarbons (C_5^+) selectivities with TOS are shown in Fig. 9. It can be seen that the selectivity to methane slowly increases while the selectivity to C_5^+ decrease with increasing TOS for all the catalysts. Comparing with Mo00/Fe catalyst, the Mo promoted catalysts produce more C_5^+ hydrocarbons while the methane selectivity is not apparently affected by the presence of Mo. Moreover, the selectivity to C_5^+ hydrocarbon products on Mo5-1/Fe catalyst is much stable during the whole reaction period. On Mo5-2/Fe catalyst, the selectivity is not stable, which continually decreases with TOS, although it is at the same level with that on Mo5-1/Fe catalyst at the initial stage of reaction.

Hydrocarbon product distributions of catalysts in detail at TOS of 100 h and 200 h are summarized in Table 5. It is shown that selectivities to light gas (C_2–C_4) and gasoline fraction (C_5–C_{11}) are markedly suppressed, whereas those to diesel and wax fractions (C_{12}^+) are improved with Mo addition. Comparing the overall hydrocarbon distributions as function of carbon number shown

Table 5
Activities and hydrocarbon selectivities of the catalysts[a].

	Mo00/Fe		Mo5-l/Fe		Mo5-2/Fe	
TOS (h)	96	192	96	192	96	215
CO conversion (mol%)	57.1	63.8	27.8	28.4	28.3	28.1
H_2 conversion (mol%)	48.9	49.9	28.8	28.2	28.8	27.6
H_2/CO exit ratio	1.4	1.5	1.2	1.2	1.2	1.2
CO_2 selectivity (mol%)	36.2	38.6	33.3	34.1	30.4	38.0
$Kp = P_{CO_2}P_{H_2}/P_{CO}/P_{H_2O}$	1.9	2.5	1.1	1.3	1.0	1.4
Hydrocarbon selectivity (wt%)						
CH_4	9.2	11.7	8.8	9.8	9.5	12.1
C_2–C_4	29.0	32.8	21.7	23.7	23.0	27.3
$C_{2-4}^=/C_{2-4}^0$	2.02	1.53	1.95	1.86	1.97	1.83
C_5–C_n	46.9	43.8	38.1	29.7	33.2	33.6
C_{12}^+	15	11.8	31.5	36.8	34.3	27.1
i-Alkane in total n-HC	3.2	2.6	5.1	7.7	9.5	5.5
i-Olefin in total n-HC (wt%)	13.0	15.0	14.3	15.1	18.4	12.4

[a] Reaction conditions: 280 °C, 1.5 MPa, $H_2/CO = 1.2$, 2000 h^{-1}.

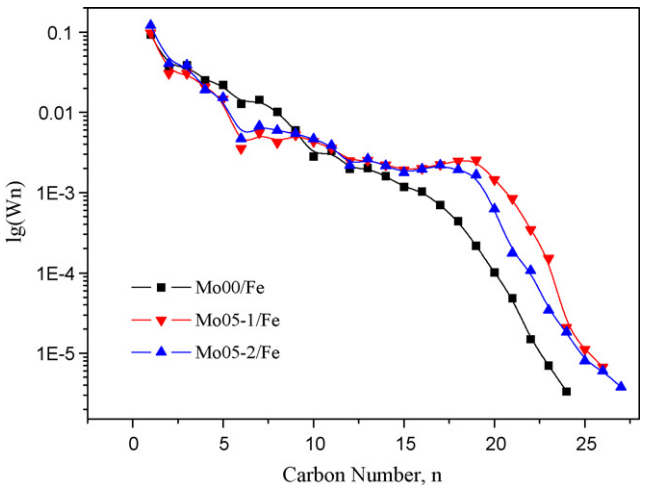

Fig. 10. Hydrocarbon distribution of the catalysts.

in Fig. 10, it can be found that Mo addition retards the formation of C_2–C_8 hydrocarbons and shifts the hydrocarbons to C_{12}^+ range.

H_2/CO ratio has a strong effect on the product selectivity. It is widely accepted that low H_2/CO ratio will facilitate the chain growth reaction on Fe catalyst [17]. As shown in Table 5, the H_2/CO exit ratios of Mo5-1/Fe and Mo5-2/Fe catalysts are lower than Mo00/Fe catalyst due to the relative low CO conversion on Mo promoted catalysts. Thus, high selectivity of heavy hydrocarbons is likely reasonable on Mo promoted catalysts. Low H_2/CO ratio only increases the chain growth probability whereas the hydrocarbon spectra of Mo-added catalysts apparently deviate from the ASF distribution. Practically all the deviations are caused by secondary reactions of the primary hydrocarbon products, such as reinsertion of olefins into the chain growth process, hydrogenation and hydrogenolysis. In this work, the deviation shows a striking similarity to the sigmoid product distribution predicted by the reinsertion/hydrogenolysis model [26]. That is, the total hydrocarbons of Mo-added catalysts are composed of higher methane, lower light hydrocarbons (C_2–C_8) and higher heavy hydrocarbons (C_9^+) relative to those of Mo-free catalyst as shown in Fig. 10. The decrease of C_2–C_8 hydrocarbons is mainly due to the reinsertion of the primary α-olefin product, which reverses the termination by β-dehydrogenation and causes an increase in the net chain growth probability [27]. The hydrogenolysis of heavy hydrocarbons plays a dominating role in the reclinate tail at high carbon numbers (C_{20}^+). It has been reported that the rates of reinsertion [28] and hydrogenolysis [29] increase exponentially with chain length. It is consistent with the maximums of the negative deviation at C_6 and the positive deviation at C_{19} observed in this work. Kuipers et al. [30] had ascribed the non-ASF product distribution to the structure-sensitive reinsertion and hydrogenolysis reactions (i.e. edge atoms can catalyze these reactions). On the one hand, the Mo-added catalysts have lower carbide content than the Mo-free catalyst in this work. The low-content phases may be highly dispersed in catalysts. Consequently, these phases have more disordered structure (more edge atoms), which enhance the reinsertion of α-olefin and the hydrogenolysis of long-chain hydrocarbons. On the other hand, Mo modified catalysts are supposed to have acidic properties [31,32] which would affect the performance of the catalysts in FTS reaction. It was reported that Mo–O–Mo clusters have strong acid sites [33] and the acidity of catalyst increased with the increasing of Mo loading. It is consistent with our NH_3-TPD experiment result (Fig. 2) which indicates that Mo addition increases the acid sites of catalyst. The secondary reactions related to the primary FTS products are mostly acid-catalyzed reactions, such as oligomerization, isomerization and catalytic cracking. Moreover, it had been reported that olefin reinsertion, oligomerization and cracking of heavy hydrocarbons could be catalyzed on acidic-zeolite and iron hybrid catalysts [34,35,7,36]. Therefore, it is reasonable for the strong fluctuations of the hydrocarbon distribution caused by the conjunction of these reactions.

4. Conclusions

Strong interaction between Fe and Mo oxides is in existence possibly due to Mo-covering the Fe-catalyzing sites and/or forming a reduction-resistant phase ($Fe_2(MoO_4)_3$), which inhibits the reduction and carburization of Fe catalyst. During the FTS process, the formation of active phases is suppressed by the Mo promoter. Thus, low FT activity was observed on Mo promoted catalysts. At the same time, Mo addition decreases the selectivity to C_2–C_8 hydrocarbons but improves the C_{12}^+ selectivity. The manner of Mo addition has an effect on the stabilization to the heavy products selectivities. During the long-time reaction, the catalyst Mo5-1/Fe, in which Mo was added by impregnation on precursor Fe/SiO_2, shows much stable product selectivity.

Acknowledgements

We thank the National Outstanding Young Scientists Foundation of China (20625620) and the National Natural Science Foundation of China (20703054, 20590361). This work is also supported by Synfuels CHINA Co., Ltd.

References

[1] F. Fischer, H. Tropsch, Brennst. Chem. 4 (1923) 276.
[2] Y. Yang, H.W. Xiang, Y.Y. Xu, L. Bai, Y.W. Li, Appl. Catal. A 266 (2004) 181.
[3] D.G. Miller, M. Moskovits, J. Phys. Chem. 92 (1988) 6081.
[4] D.B. Bukur, D. Mukesh, S.A. Patel, Ind. Eng. Chem. Res. 29 (1990) 194.
[5] L. Bai, H.W. Xiang, Y.W. Li, Y.Z. Han, B. Zhong, Fuel 81 (2002) 1577.
[6] T.Z. Li, Y. Yang, C.H. Zhang, X. An, H.J. Wan, Z.C. Tao, H.W. Xiang, Y.W. Li, F. Yi, B.F. Xu, Fuel 86 (2007) 921.
[7] F.G. Botes, W. Böhringer, Appl. Catal. A 267 (2004) 217.
[8] A. Martínez, C. López, Appl. Catal. A 296 (2005) 251.
[9] J.F. Schultz, F.S. Karn, R.B. Anderson, U.S. Bureau of Mines, Report (1967) 6974.
[10] C.B. Murchison, D.A. Murdick, Hydrocarbon Process. 60 (1981) 159.
[11] O.W. Dun, E. Gulari, K.Y.S. NG, Appl. Catal. 15 (1985) 247.
[12] R.V. Belosudov, S. Sakahara, K. Yajima, S. Takami, M. Kubo, A. Miyamoto, Catal. Today 189 (2002) 245.
[13] R.B. Levy, M. Boudart, Science 181 (1973) 547.
[14] I. Kojima, E. Miyazaki, Y. Inoue, I. Yasumori, J. Catal. 73 (1982) 128.
[15] E. Iglesia, J. Baumgartner, F.H. Ribeiro, M. Boudart, J. Catal. 131 (1991) 523.
[16] W.P. Ma, E.L. Kugler, J. Wright, D.B. Dadyburjor, Energy Fuels 20 (2006) 2299.
[17] C.H. Zhang, Y. Yang, B.T. Teng, T.Z. Li, H.Y. Zheng, H.W. Xiang, Y.W. Li, J. Catal. 237 (2006) 405.
[18] D. Lin, K.D. Chen, Y. Chen, J. Solid State Chem. 129 (1997) 30.
[19] P. Arnoldy, J.C.M. de Jonge, J.A. Moulijn, J. Phys. Chem. 89 (1985) 4517.
[20] K.V.R. Chary, K.R. Reddy, G. Kishan, J.W. Niemantsverdriet, G. Mestl, J. Catal. 226 (2004) 283.
[21] Y. Jin, A.K. Datye, J. Catal. 196 (2000) 8.
[22] M. Shimokawabe, R. Furuichi, T. Ishii, Thermochim. Acta 28 (1979) 287.
[23] M.J. Tiernan, P.A. Barnes, G.M.B. Parkes, J. Phys. Chem. B 105 (2001) 220.
[24] H. Zhang, J. Shen, X. Ge, J. Solid State Chem. 117 (1995) 127.
[25] N. Lohitharn, J.G. Goodwin Jr., E. Lotero, J. Catal. 255 (2008) 104.
[26] G.A. Huff, C.N. Satterfield, J. Catal. 85 (1984) 370.
[27] S. Novak, R.J. Madon, H. Suhl, J. Chem. Phys. 74 (1981) 6083.
[28] R.J. Madon, S.C. Reyes, E. Iglesia, J. Phys. Chem. 95 (1991) 7795.
[29] E.W. Kuipers, I.H. Vinkenburg, H. Oosterbeek, J. Catal. 152 (1995) 137.
[30] E.W. Kuipers, C. Scheper, J.H. Wilson, I.H. Vinkenburg, H. Oosterbeek, J. Catal. 158 (1996) 288.
[31] E. van Steen, E.L. Viljoen, J. van de Loosdrecht, M. Claeys, Appl. Catal. A 335 (2008) 56.
[32] G.L. Schrader, C.P. Cheng, J. Phys. Chem. 87 (1983) 3675.
[33] E. van Steen, E.L. Viljoen, M. Claeys, J. Mol. Catal. A 266 (2007) 254.
[34] A. Shamsi, V.U.S. Rao, R.J. Gormley, R.T. Obermyer, R.R. Schehl, J.M. Stencel, Appl. Catal. 27 (1986) 55.
[35] A. Martínez, C. López, Appl. Catal. A 294 (2005) 251.
[36] A.N. Pour, Y. Zamani, A. Tavasoli, S.M.K. Shahri, S.A. Taheri, Fuel 87 (2008) 2004.